Available online at www.dergipark.org.tr/en

INTERNATIONAL ADVANCED RESEARCHES and ENGINEERING JOURNAL

Journal homepage: www.dergipark.org.tr/en/pub/iarej

e-ISSN: 2618-575X

International Open Access

Volume 08
Issue 03

December, 2024

Research Article

Simulation of fuzzy logic and PI control methods on a bridgeless isolated SEPIC converter for electric vehicle chargers

Alperen Uğurluoğlu [a]* ***and Ahmet Karaarslan*** [a]

[a] *Ankara Yıldırım Beyazıt University, Institute of Science, Department of Electrical and Electronics, 6010, Keçiören/Ankara*

ARTICLE INFO

Article history:
Received 13 June 2024
Accepted 12 December 2024
Published 20 December 2024

Keywords:
BL SEPIC
Fuzzy controller
PFC
PI controller
THD

ABSTRACT

Studies in literature and the increasing trend of electrification show that electric vehicles (EVs) will become more widespread in the future. However, the growing demand for EV chargers causes an overload on the grid. Furthermore, EV chargers generate power factor distortion and harmonics, which contaminate the grid and lower the quality of power. Therefore, power factor correction (PFC) is applied by EV chargers to mitigate the harmonics. As defined in the IEC 61000-3-2 standard, the total harmonic distortion (THD) shall be less than 5%. In this study, a better PFC operation is achieved with the proposed bridgeless isolated single ended primary inductor converter (BL SEPIC) topology as an EV charger instead of conventional converter topologies that have diode bridge rectifiers (DBR). Also, the study has better THD outputs as compared with the similar bridgeless (BL) topologies in literature thanks to the simulated control methods of the proportion-integration (PI) and fuzzy control. Moreover, these control methods are compared with each other in terms of THD suppression performance, stability, robustness, and computational effort. The results showed that the fuzzy controller has advantages of stability and robustness against the transient conditions, input voltages and load changes for THD suppression while the PI controller has better THD results only for steady state operation with nominal input voltage and full load conditions. The implemented PI and fuzzy controllers are simulated in a MATLAB Simulink environment.

1. Introduction

Nowadays, the increasing amount of greenhouse gas emissions leads people to seek out greener fuels, such as electricity, instead of fossil fuels. Thus, electric vehicles have started to be popular instead of internal combustion engines. [1] Thanks to battery energy storage (BES) systems, it is possible to store electrical energy in transport vehicles. [2] However, BES systems require EV battery charging units, whether on-board or off-board. [3] Moreover, the increasing number of EV chargers burdens the power grid. Therefore, the grid power quality drops since the EV chargers produce harmonics and have a poor power factor. Hence, the EV charging system shall be designed to produce a high-power factor and low harmonics and provide clean power utilization when it is connected to the grid. [4-7]

The input power quality (PQ) indices shall be maintained by the charger in accordance with the IEC 61000-3-2:2018 standard. [8-9] Nevertheless, traditional EV battery chargers use a filtered output from a diode bridge rectifier (DBR), which produces harmonics, to draw power from an alternative current (AC) supply. [10-11] According to the reviews in the literature, the THD produced by the converters that use DBR is in the range of 15% to 80%. [12] The buck and boost topologies that use DBR are the most preferable solutions for low power applications due to low-cost effectiveness and simplicity. [13-14, 28] However, they have poor PFC operation and high conduction losses for high power applications because of the poor controller algorithm and the number of components in the circuitry. In contrast, the buck-boost topologies have better PFC operation since they have both step-up and step-down features to control the output, but these topologies are not sufficient to fully suppress the harmonics as well. [15]

Several other PFC topologies in the literature utilize DBR structures such as CUK, zeta and SEPIC converters. [16] These topologies have better PFC operation as compared with buck boost topologies, and their structure allows to reduce ripples. On the other hand, the size of these circuits is bulkier, especially in CUK and zeta converters due to the

* Corresponding author. Tel.: *+90-554-983-0402*.
E-mail addresses: alperen.ugurluoglu@gmail.com *(Alperen UĞURLUOĞLU)*, akaraarslan@gmail.com *(Ahmet KARAARSLAN)*
ORCID: 0000-0001-8038-5729 *(Alperen UĞURLUOĞLU)*, 0000-0001-6475-4539 *(Ahmet KARAARSLAN)*
DOI: 10.35860/iarej.1501059

extra filtering stage and the need for high voltage DC link capacitors. [17] Also, the current and voltage stresses are high due to their single stage and non-interleaved structures, especially for the SEPIC converter. [18] Beside that, the full bridge and inductor-inductor-capacitor (LLC) converter topologies in the literature are preferable due to their high-power density, high efficiency and low electromagnetic interference (EMI). [19-21] However, the cost effectiveness of these topologies is very low, and these topologies offer complex control systems for PFC operation. In addition, the LLC topologies are used with DBR or other PFC converters. If the DBR structure is used, the LLC topology becomes simpler and smaller in size, but the power loss increases. If another PFC converter is used, the power loss drops remarkably, but the cost and size also increase. [22]

On the other hand, high harmonic suppression, low EMI and better PFC operation can be achieved by interleaved AC to direct current (DC) PFC converter topologies such as boost, SEPIC and flyback. [22-23] In addition, the losses and heating problems are reduced since each switching component handles only the half cycle of the ac mains. However, the reduction of losses, heat problems and THD is limited due to the existence of DBR in the topologies.

In literature, interleaved converters without DBR are found such as isolated interleaved Luo and SEPIC converters. [16] The synchronous rectifier and interleaved structure provide lower voltage and current stresses with high efficiency. In addition, higher PFC performance, low THD and unity PF are obtained without any extra filtering circuit. However, the component and switching element counts require complex control methods and cause large size. In literature, several topologies with reduced component count are found. [24] These topologies have features of less component count, simpler control with high efficiency and low THD. The BL SEPIC topologies among these converters are found to be a good solution due to their lower component count, simple control, high efficiency and low THD performance. [27,38]

Furthermore, the controller methods of EV chargers are investigated to provide better PFC operation to suppress the THD that reduces the power quality of the grid, as given in Figure 1. [28-30] It is seen that there are two groups of control methods, which are linear and non-linear methods. The linear methods of PI and proportion-integration-derivation (PID) controllers are the widely used and conventional methods in literature due to their simplicity and applicability. [31-32] On the other hand, the tuning process of these linear controllers requires difficult techniques such as assumption based algorithms, mathematical model calculations or intelligent tuning algorithms. The Ziegler-Nichols method, state space modeling, genetic algorithm or neural network algorithms are several techniques for tuning a linear controller. [29, 33-34] In addition, the linear controllers have deficiencies while controlling the converters in different working conditions such as transient operations, different input voltage levels and output load changes. The stability and robustness of the linear controllers decrease as getting away from the tuned region. At that point, the non-linear control methods have better performance for changing conditions such as sliding mode, model predictive and fuzzy logic controllers. [35] However, sliding mode and model predictive control methods still require mathematical models of the controlled topology, whereas the fuzzy logic controller provides a linguistic base control method while the non-linear feature is preserved. [36-37]

In this study, a BL SEPIC converter is proposed for better PFC operation and lower THD performance. [38] The proposed converter is controlled with PI and fuzzy controllers to compare their PFC operation and THD mitigation performance. The low THD performance is achieved excellently with both linear PI control and the nonlinear method of fuzzy control. [39] Even if the PI controller has better performance for its tuned steady state operation of nominal input voltage and full load condition, the fuzzy controller shows better PFC operation when transient operations, input voltage and output load changes are simulated. Therefore, the fuzzy controller has better stability and robustness for a wide operating condition such as input voltage swings and output load changes. By using MATLAB Simulink, controller systems are implemented and simulated on the BL SEPIC converter.

The theoretical calculations and the operating principle are described in part 2. In part 3, the transient and steady state operations of the BL SEPIC are observed using the PI and fuzzy controller.

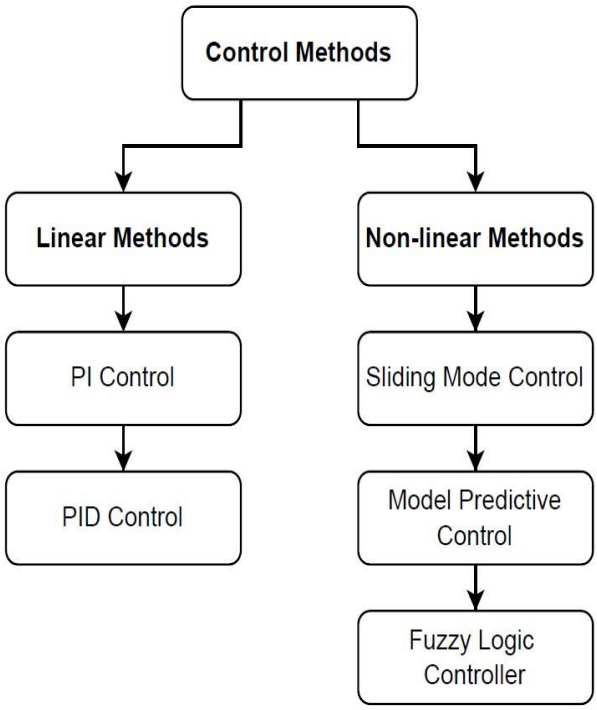

Figure 1. Classification of control methods

In addition, the BL SEPIC topology is also simulated with cases of input voltage and output load fluctuations to obtain the transient performance of the PI and fuzzy controllers. The input voltage fluctuation range is determined as 230±10% V_{rms} according to the standard of IEC 60038:2009 [40]. The operating principle of the PI controller is detailed, and the simulation results are shown in part 3.1. On the other hand, the operating principle and the simulation results of the fuzzy controller are described in part 3.2. The summary of this paper are given in the conclusion chapter.

2. Proposed Topology

The proposed topology is shown in Figure 2. The BL SEPIC topology includes two individual isolated SEPIC topologies. One of them regulates the positive half cycles of the AC input voltage, and the other regulates the negative half cycles. The average of one period of the positive or negative cycle of input voltage, V_{inav}, is obtained with Equation (1). Then, the dc output voltage, V_{dc}, is obtained with Equation (2).

$$V_{inav} = \frac{2\sqrt{2} * V_{in}}{\pi} \quad (1)$$

$$V_{dc} = \frac{n * V_{inav} * D}{(1-D)} \quad (2)$$

The BL SEPIC converter has two transformers (L_{m1}, L_{m2} = 155 µH, also with turns ratio $n = N_2/N_1$ = 1.305) and one inductor (L_i = 630 µH) for isolated energy transfer and storing energy, respectively. The magnetizing inductor values of the transformers, $L_{m1,2}$,are obtained with Equation (3). The input inductor, L_i, is calculated with Equation (4).

$$L_i = \frac{V_{in} * D}{2 * I_{in} * f} \quad (3)$$

$$L_{m1,2} = \left(\frac{N_1}{N_2}\right)^2 * \frac{V_{dc} * (1-D)^2}{2 * D * f_s * I_{dc}} \quad (4)$$

There are four switching elements (S_1, S_2, D_1 and D_2) to modulate the passive elements. Also, three capacitors (C_1, C_2 = 1 µF, C_{dc} = 5.8 mF) and a resistive load (R_{dc} = 5.6 Ω) are used in the BL SEPIC topology as passive elements. The primary capacitors, $C_{1,2}$, are calculated with Equation (5), while the output capacitor, C_{dc}, is calculated with Equation (6).

$$C_{1,2} = \frac{N_2 * V_{dc} * D}{N_1 * (\Delta V_{c1,2} * f_s * R_{dc})} \quad (5)$$

$$C_{dc} = \frac{I_{dc}}{2 * \omega * \Delta V_{dc}} \quad (6)$$

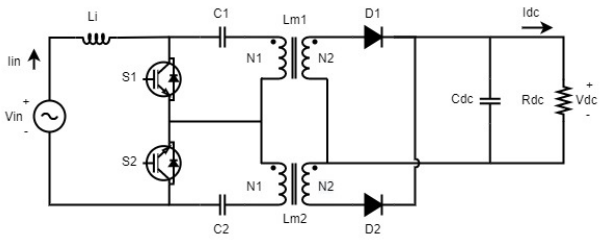

Figure 2. Proposed BL SEPIC topology

The converter is designed for 760 W output at 65 V_{dc} and 220 V_{rms} input voltage, while switching frequency is 50 kHz.

2.1. Operation Principle

Positive Half Cycle Operation:

The S_1 switch is initiated in the on state when the BL SEPIC is in the positive half-cycle of the AC supply. The L_i inductor and the transformer are charged in this state, while the output is fed by the C_{dc} Capacitor. Then, the BL SEPIC topology switches to the off state by turning off the S_1. The L_i inductor and the transformer are discharged in this state to feed the output. The on and off cycles are shown in Figure 3 (a) and Figure 3 (b), respectively.

Negative Half Cycle Operation:

The S_2 switch is initiated in the on state when the BL SEPIC is in the negative half-cycle of the AC supply. The L_i inductor and the transformer are charged in this state, while the output is fed by the C_{dc} Capacitor. Then, the BL SEPIC is altered from an on state to an off state by turning off the S_2. The L_i inductor and the transformer are discharged in this state to feed the output. The on and off cycles are shown in Figure 4 (a) and Figure 4 (b), respectively.

3. Results

BL SEPIC is set up in the Simulink environment. The passive components are adjusted to pre-calculated values. The THD of the input current is calculated with the help of the MATLAB Simulink fast fourier transform (FFT) analysis tool, which is based on Equation (7) for THD calculations. [41]

$$THD = \frac{\sqrt{\sum_{n=2}^{\infty}(I_n)^2}}{I_{fundamental}} \quad (7)$$

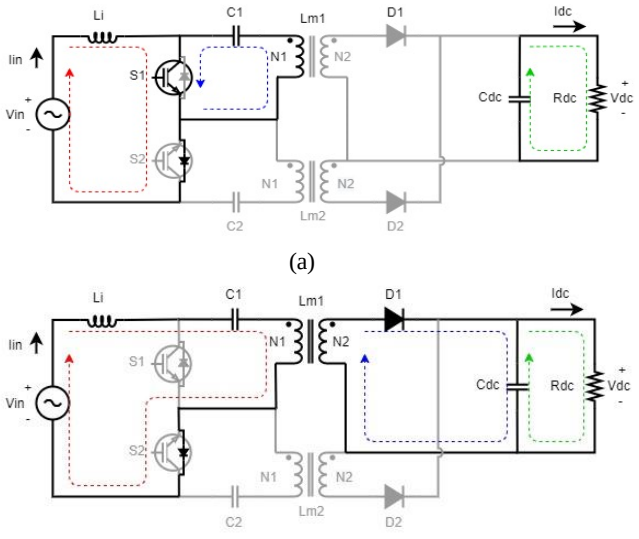

(a)

(b)

Figure 3. Positive half cycle operating states of BL SEPIC a) S1 switch is turned-on b) S1 switch is turned-off

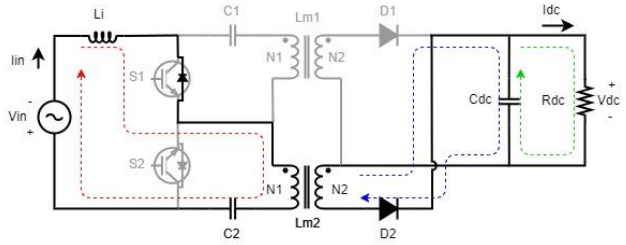

(a)

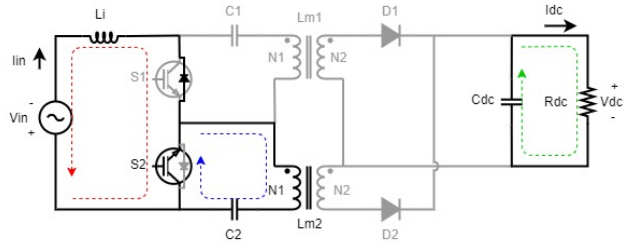

(b)

Figure 4. Negative half cycle operating states of BL SEPIC a) S2 switch is turned-on b) S2 switch is turned-off

3.1. PI Controller Method

The PI controller employs an error input and outputs a duty value. A proportional constant (K_p) is used to multiply the error, and a constant is used to integrate the error (K_i). The sum of multiplication and integration results is the duty output as seen in Equation (8). [43]

$$G_{pi} = K_p + \frac{K_i}{s} = \frac{K_p * s + K_i}{s} \tag{8}$$

As shown in Figure 5, the implemented PI controller block has one PWM output and three inputs: output voltage, V_{ofb}, input voltage, V_{infb}, and input current, I_{fb}. The PWM output of the controller drives two insulated gate bipolar transistor (IGBT) switches. Initially, a DC voltage error, V_{dce}, is calculated by comparing V_{ofb} to the reference output voltage, V_{oref}. The PI voltage controller amplifies the error to obtain the reference input current magnitude, I_{inref}. In the event of an overshoot case at the output, the PI voltage controller has a reset function to suppress the overshoots. The PI controller cannot react to instant load changes due to its integral coefficient. Therefore, the reset function provides a rapid decrease in the PI controller output. Thus, the overshoot is suppressed.

To synchronize I_{inref} with the grid voltage frequency, V_{infb} is filtered through a phase locked loop (PLL) block to have a grid frequency. In the next step, I_{fb} is compared with I_{inref} to get the current error, I_{inerr}. A duty magnitude is calculated from the I_{inerr} by using a PI current controller to produce a PWM signal by comparing it with a 50 kHz sawtooth signal.

The K_p and K_i parameters of both PI controllers need to be properly tuned for steady operation of the BL SEPIC. Therefore, the mathematical model of the BL SEPIC is obtained to find the proper PI controller parameters by applying the studies in the literature [33-34, 42]. Then, a transfer function (TF) is calculated and used for tuning the parameters.

On state equations:

$$\frac{dI_{L1}}{dt} = \frac{1}{L1}(V_{in}) \tag{9}$$

$$\frac{dV_{C1}}{dt} = \frac{1}{C1} * (-I_{Lm}) \tag{10}$$

$$\frac{dI_{Lm}}{dt} = \frac{1}{Lm}(V_{C1}) \tag{11}$$

$$\frac{dV_{Co}}{dt} = \frac{1}{Co}\left(-\frac{V_{Co}}{R}\right) \tag{12}$$

Off state equations:

$$\frac{dI_{L1}}{dt} = \frac{1}{L1}\left(V_{in} + \frac{V_{Co}}{n} - V_{C1}\right) \tag{13}$$

$$\frac{dV_{C1}}{dt} = \frac{1}{C1} * (I_{L1}) \tag{14}$$

$$\frac{dI_{Lm}}{dt} = \frac{1}{Lm}\left(-\frac{V_{Co}}{n}\right) \tag{15}$$

$$\frac{dV_{Co}}{dt} = \frac{1}{Co}\left(\frac{I_{L1} + I_{Lm}}{n} - \frac{V_{Co}}{R}\right) \tag{16}$$

At the start, only the positive half cycle operation is considered for transfer function calculation since the negative side has similar behavior. The transfer function is obtained by calculating the state space and output equations. The state space and output equations are obtained from the on state and off state equations given above. Then, these equations are represented in a matrix form. The state space equations are given in equations (18) and (20). The output equations are equal and given in equations (22).

$$x^* = A_1 * x + B_1 * u \tag{17}$$

$$\begin{bmatrix} I_{L1}^* \\ V_{C1}^* \\ I_{Lm}^* \\ V_{Co}^* \end{bmatrix} = \begin{bmatrix} 0 & 0 & 0 & 0 \\ 0 & 0 & -\frac{1}{C1} & 0 \\ 0 & \frac{1}{Lm} & 0 & 0 \\ 0 & 0 & 0 & -\frac{1}{RCo} \end{bmatrix} * \begin{bmatrix} I_{L1} \\ V_{C1} \\ I_{Lm} \\ V_{Co} \end{bmatrix} + \begin{bmatrix} \frac{1}{L1} \\ 0 \\ 0 \\ 0 \end{bmatrix} * V_{in} \tag{18}$$

$$x^* = A_2 * x + B_2 * u \tag{19}$$

$$\begin{bmatrix} I_{L1}^* \\ V_{C1}^* \\ I_{Lm}^* \\ V_{Co}^* \end{bmatrix} = \begin{bmatrix} 0 & -\frac{1}{L1} & 0 & \frac{1}{nL1} \\ \frac{1}{C1} & 0 & 0 & 0 \\ 0 & 0 & 0 & -\frac{1}{nLm} \\ \frac{1}{nCo} & 0 & \frac{1}{nCo} & -\frac{1}{RCo} \end{bmatrix} * \begin{bmatrix} I_{L1} \\ V_{C1} \\ I_{Lm} \\ V_{Co} \end{bmatrix} + \begin{bmatrix} \frac{1}{L1} \\ 0 \\ 0 \\ 0 \end{bmatrix} * V_{in} \tag{20}$$

The calculated output equations for both on and off states are equal.

$$y = C_1 * x + D_1 * u = C_2 * x + D_2 * u \tag{21}$$

$$\begin{bmatrix} Vo \\ Io \\ Iin \end{bmatrix} = \begin{bmatrix} 0 & 0 & 0 & 1 \\ 0 & 0 & 0 & \frac{1}{R} \\ 1 & 0 & 0 & 0 \end{bmatrix} * \begin{bmatrix} I_{L1} \\ V_{C1} \\ I_{Lm} \\ V_{Co} \end{bmatrix} + [0] * V_{in} \tag{22}$$

These matrix representations are used to obtain an average matrix model that also represents the large signal model of BL SEPIC. The average model is calculated with the equations from (23) to (26), and the calculated matrix forms are written in equation (27) and (28) format.

$$\mathrm{A} = [A_1 * (d) + A_2 * (1 - d)] \tag{23}$$

$$B = [B_1 * (d) + B_2 * (1-d)] \quad (24)$$

$$C = [C_1 * (d) + C_2 * (1-d)] \quad (25)$$

$$D = [D_1 * (d) + D_2 * (1-d)] \quad (26)$$

Moreover, the small signal model is obtained by applying the equation (27) and (28). The final model is used to calculate the transfer function of the BL SEPIC.

The small signal state space equation is given below.

$$\dot{\hat{x}} = A * \hat{x} + B * \hat{u} + [(A_1 - A_2)(X) + (B_1 - B_2)(U)] * (\hat{d}) \quad (27)$$

The small signal output equation is given below.

$$\hat{y} = C * \hat{x} \quad (28)$$

The final mathematical state space model of the system is given below. The obtained small signal model contains passive component equations and also input parameters of $\hat{v}_{in}$ and $\hat{d}$.

$$\begin{bmatrix} \dot{\hat{\imath}}_{L1} \\ \dot{\hat{v}}_{C1} \\ \dot{\hat{\imath}}_{Lm} \\ \dot{\hat{v}}_{Co} \end{bmatrix} = \begin{bmatrix} 0 & \frac{D-1}{L_1} & 0 & \frac{D-1}{nL_1} \\ \frac{1-D}{C_1} & 0 & \frac{-D}{C_1} & 0 \\ 0 & \frac{D}{L_m} & 0 & \frac{D-1}{nL_m} \\ \frac{1-D}{nC_o} & 0 & \frac{1-D}{nC_o} & -\frac{1}{RC_o} \end{bmatrix} \begin{bmatrix} \hat{\imath}_{L1} \\ \hat{v}_{C1} \\ \hat{\imath}_{Lm} \\ \hat{v}_{Co} \end{bmatrix} + \begin{bmatrix} \frac{1}{L_1} \\ 0 \\ 0 \\ 0 \end{bmatrix} \hat{v}_{in} + \begin{bmatrix} \frac{nV_{C1}-V_{Co}}{nL_1} \\ \frac{-I_{L1}-I_{Lm}}{C_1} \\ \frac{nV_{C1}+V_{Co}}{nL_m} \\ \frac{-I_{L1}-I_{Lm}}{nC_o} \end{bmatrix} \hat{d} \quad (29)$$

The mathematical output model of the system is given below. The output model contains Vo, Io and Iin parameters.

$$\begin{bmatrix} Vo \\ Io \\ Iin \end{bmatrix} = \begin{bmatrix} 0 & 0 & 0 & 1 \\ 0 & 0 & 0 & \frac{1}{R} \\ 1 & 0 & 0 & 0 \end{bmatrix} * \begin{bmatrix} I_{L1} \\ V_{C1} \\ I_{Lm} \\ V_{Co} \end{bmatrix} + [0] * V_{in} \quad (30)$$

The equations below are used to calculate the TF of the BL SEPIC PI controllers. Then, the MATLAB Sisotool application is used to obtain PI parameters.

$$G_{vod} = \frac{\hat{v_o}}{\hat{d}} = C * [s * I - A]^{-1} * [B] = \frac{-3.859e8 * s^2 + 5.503e11 * s - 1.183e17}{s^4 + 96.62 * s^3 + 7.909e7 * s^2 + 7.381e9 * s + 6.11e14} \quad (31)$$

$$G_{iind} = \frac{\hat{i_{in}}}{\hat{d}} = C * [s * I - A]^{-1} * [B] = \frac{4.787e5 * s^3 + 8.314e8 * s^2 - 8.939e13 * s - 5.788e15}{s^4 + 96.62 * s^3 + 7.909e7 * s^2 + 7.381e9 * s + 6.11e14} \quad (32)$$

The voltage and the input current PI controllers are tuned with the parameters given in Table 1.

Table 1. PI control parameters

Voltage Controller		Input Current Controller	
K_p	K_i	K_p	K_i
4.7118e-05	1.49269824	1.1093	6.26359234

As shown in Figure 6 (a) and Figure 6 (b), the rms of the AC input voltage is 230 V_{rms} and the output voltage, V_o, is 65 V. The peak of the AC input current is 5 A. The THD level is 1.08%, as is depicted in Figure 7, so the input current is nearly a pure sine wave. Also, the full load current of 12 A is set on the output.

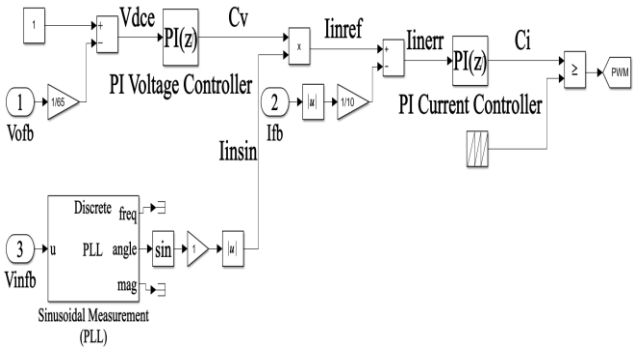

Figure 5. PI controller of the proposed study

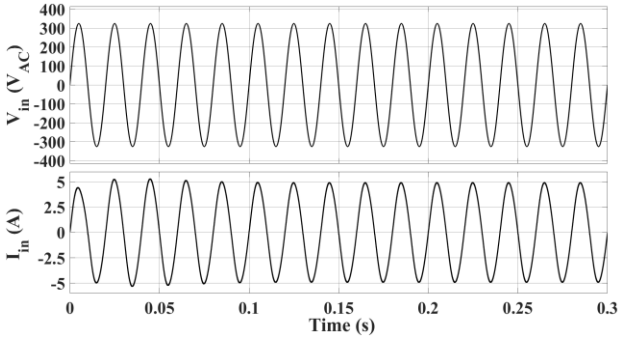

(a)

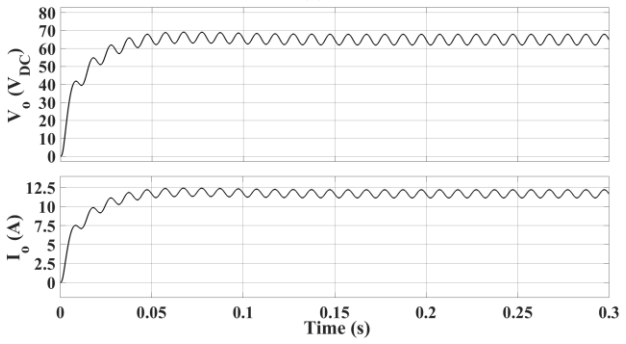

(b)

Figure 6. a) Steady state input voltage and current of PI controlled BL SEPIC, b) Steady state output voltage and current of PI controlled BL SEPIC.

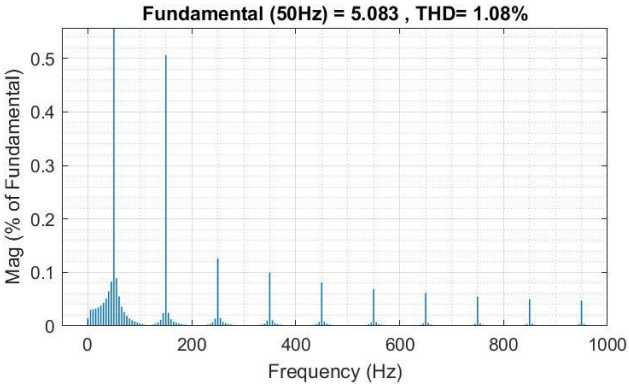

Figure 7. THD result of PI controller for a steady state operation

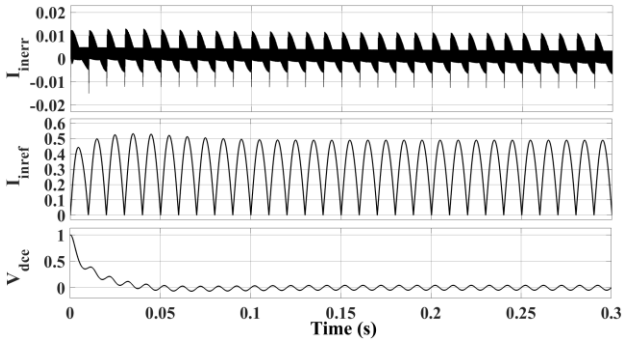

Figure 8. Current error, current reference, and voltage error signals of PI controller.

The PI controller signals are observed to understand the controller operation, as seen in Figure 8. The V_{dce} settled around zero by starting from one in 38 milliseconds. The rectified I_{inref} is obtained with a peak unit of 0.5 that corresponds to 5 A current at the input. In addition, the rectification is applied to I_{inref} because of the positive duty ratio. On the other hand, the deviation of the input current error, I_{inerr}, from zero is observed. The deviation is captured as 0 ± 0.015A. The obtained deviation also shows the magnitude of the harmonics.

The PI controller is simulated for both the input voltage and output load fluctuation cases. As shown in Figure 9, the input voltage fluctuation case is simulated within the previously established range, which is the maximum voltage of 253 V_{rms}, the minimum voltage of 207 V_{rms} and the nominal voltage of 230 V_{rms}, respectively. After the input voltage fluctuation range is applied to the BL SEPIC converter, the change in input current is observed as 4.5 A, 5.5 A and 5 A, respectively. As depicted in Figure 9 (b), the full load operation is applied at the output, and a steady state current of 12 A is obtained. At the instantaneous changes in input voltage, a drop of 11 A and a rise of 12.5 A are observed in the output current. On the other hand, the output voltage drops to 60 V_{dc} and increases up to 70 V_{dc}. In addition, it is seen that the output reaches the steady state within 50 milliseconds after each change, and any overshoot case is not observed by the PI voltage controller, therefore, the reset function is inactive.

The THD level of the PI controller is 1.98% when the input voltage is the maximum of 253 V_{rms}, as seen in Figure 10 (a). Also, the THD is 1.64% for the minimum of 207 V_{rms}, as seen in Figure 10 (b). As a result, the input voltage fluctuations are suppressed by the PI controller, and the THD is within the limits that are specified in the standard.

The output load fluctuation case is simulated for the PI controller, as shown in Figure 11. At the output voltage of 65 V_{dc}, the full load of 12 A, the quarter load of 3 A, and the half load of 6 A are applied, respectively. The rapid transition from the full load to the quarter load results in an overshoot at the output. After the predefined 72 V_{dc} overshoot level is exceeded, the reset feature of the PI voltage controller is triggered by the resultant overshoot, and the I_{inref} output is dropped to its initial state. Thus, the overshoot is suppressed, and the output reaches its steady state. Finally, the half load of 6 A is applied to the PI controller. As shown in Figure 11 (b), a drop of 60 V_{dc} at the output voltage is observed for less than 50 milliseconds, then reaches its steady state.

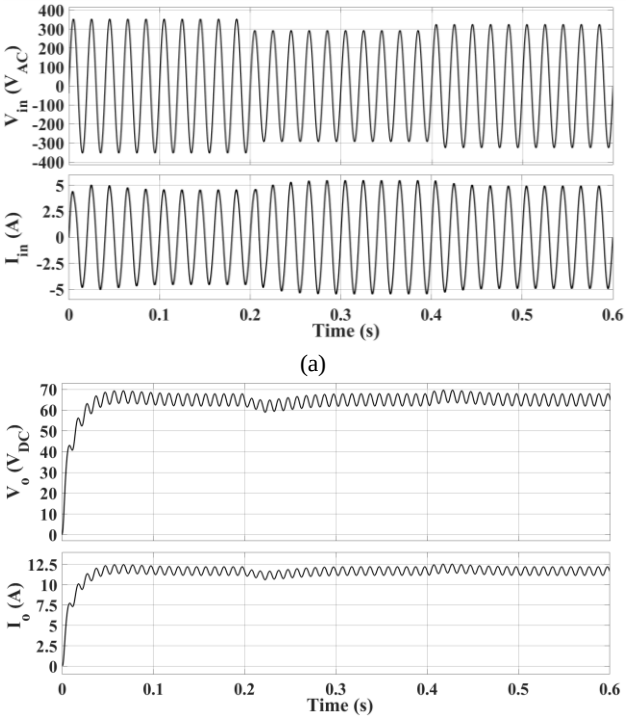

Figure 9. The input voltage fluctuation is applied to PI, a) Input voltage and current, b) Output voltage and current

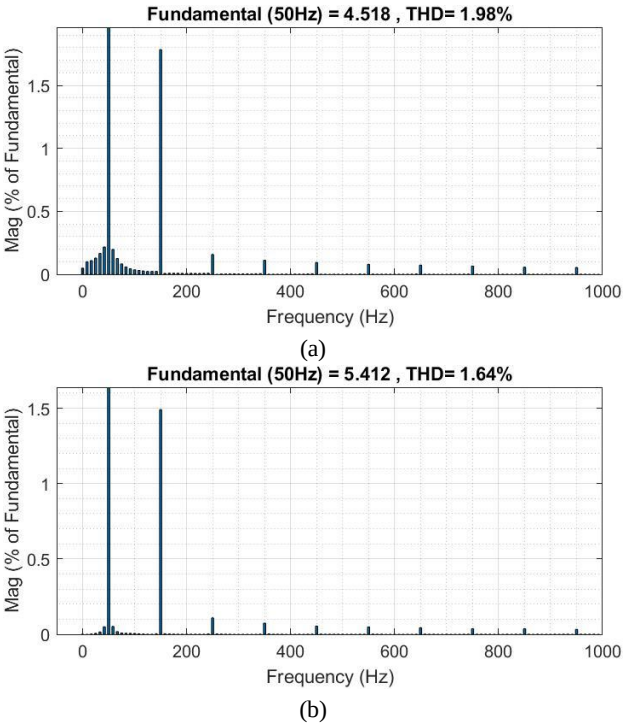

Figure 10. a) Transient THD when the input voltage is 253 V_{rms}, b) Transient THD when the input voltage is 207 V_{rms}

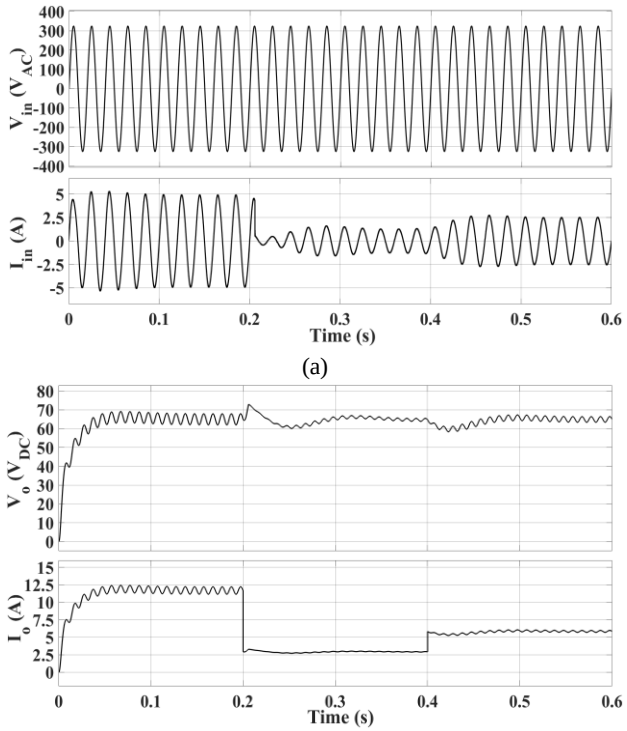

(a)

(b)

Figure 11. a) Input voltage and current results of PI controller when the output load fluctuation is applied, b) Output voltage and current results of PI controller when the output load fluctuation is applied

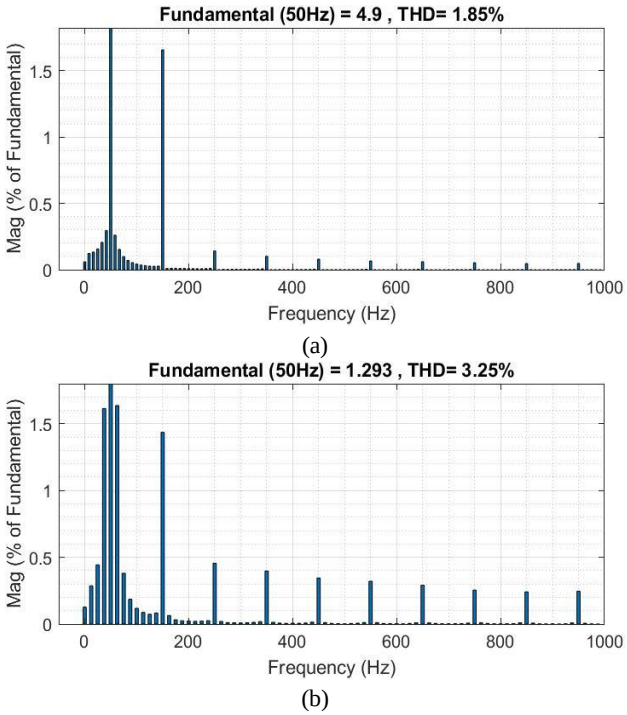

(a)

(b)

Figure 12. a) Transient THD result of PI controller at full load, b) Transient THD result of PI controller at quarter load

The THD results of the PI controller are given in Figure 12 (a) and Figure 12 (b). The full load application provides the minimum THD of 1.85%, while the quarter load application provides the maximum THD of 3.25%. As a result, the THD level is again compliant with the standard.

3.2. Fuzzy Controller Method

In the fuzzy controller, the input current PI controller is replaced with a fuzzy controller while the output voltage PI controller is the same, as shown in Figure 13. Since the fuzzy controller is based on linguistic qualifiers and has no system model, the studies in the literature are taken as initial references to define input and output membership (MS) functions. [36-37] Upon this, the input and output MS functions are tuned to get the optimal performance. Thus, each fuzzy controller input MS is defined on an error range in between -0.1 and 0.1 to make the system react faster to error changes, as shown in Figure 14. [44-45] Also, each output MS is defined over a duty output value range in between 0 and 1 to limit the duty output, as shown in Figure 15. The purpose is to set a proper duty output by relating the input and output MS functions to each other. Therefore, a rule table is assigned, and related memberships are given in Table 2. On the other hand, the defined input and output MS functions are adjusted with the system parameters, as shown in Table 2.

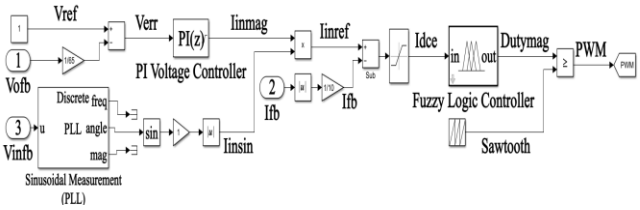

Figure 13. Fuzzy controller of proposed topology

Table 2. Rules table of fuzzy logic

Rules Table	
Input MS	Output MS
3L_N	3L
2L_N	2L
L_N	L
M	M
H_P	H
2H_P	2H
3H_P	3H

Table 3. Membership parameters of fuzzy logic

Fuzzy Membership Parameters			
Input MS		Output MS	
3L_N	[-0.16 -0.14 -0.015 0]	3L	[0 0.01 0.025]
2L_N	[-0.04 -0.005 0]	2L	[0.01 0.03 0.045]
L_N	[-0.015 -0.002 0]	L	[0.02 0.05 0.06]
M	[0 0.002 0.015]	M	[0.27 0.3 0.33]
H_P	[0 0.002 0.015]	H	[0.88 0.9 0.98]
2H_P	[0 0.005 0.04]	2H	[0.917 0.942 0.99]
3H_P	[0 0.02 0.17 0.19]	3H	[0.917 0.942 0.99]

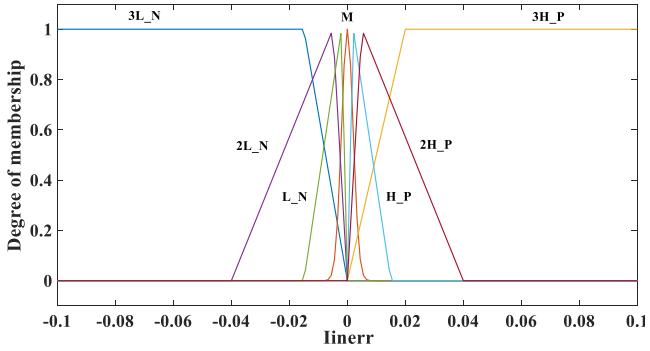

Figure 14. Input memberships of fuzzy controller

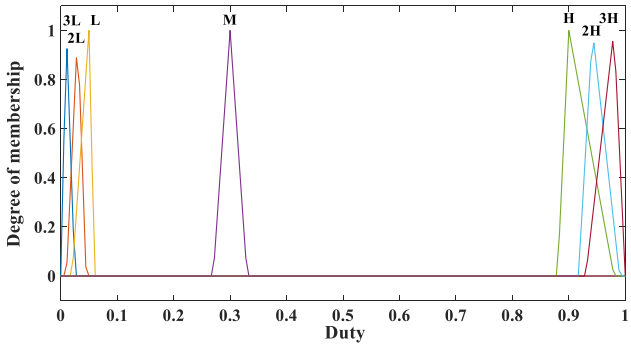

Figure 15. Output memberships of fuzzy controller

As shown in Figure 16 (a) and Figure 16 (b), The peak of the AC input voltage is 230 V_{rms}, and the output voltage, V_o, is 65 V. The peak of the AC input current is 5 A. The THD level is 1.33%, as depicted in Figure 17, so the input current is nearly a pure sine wave.

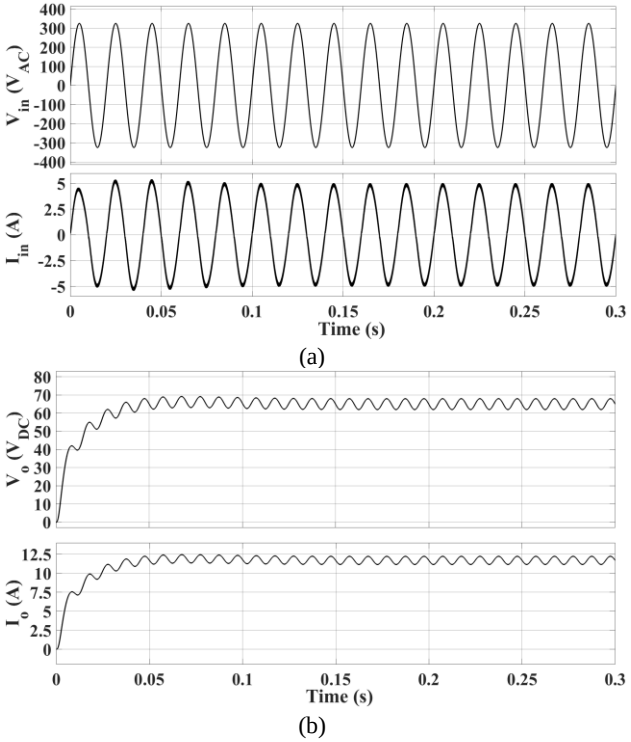

(a)

(b)

Figure 16. a) Steady state input voltage and current results of the fuzzy controlled topology, b) Steady state output voltage and current results of the fuzzy controller

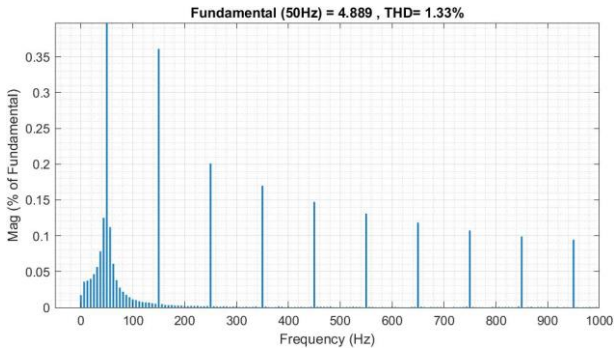

Figure 17. THD result of fuzzy method for a steady state operation

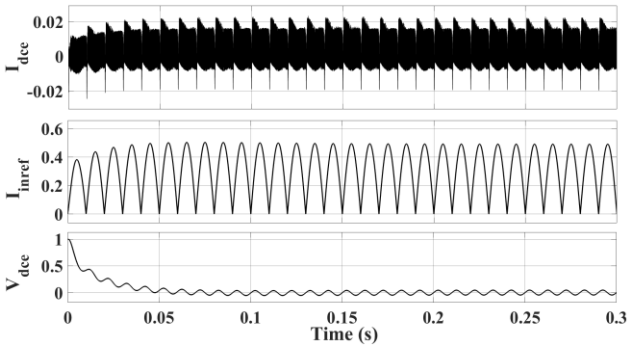

Figure 18. I_{dce}, I_{inref}, and V_{dce} signals of fuzzy controller.

The input current error, I_{dce}, the input reference current, I_{inref}, and the DC voltage error, V_{dce}, signals of the fuzzy controller are obtained, as shown in Figure 18. The V_{dce} reaches to steady state in 37 milliseconds. The I_{inref} signal is obtained with a peak of 0.5. The deviation of the I_{dce} signal is captured as 0 ± 0.02 A.

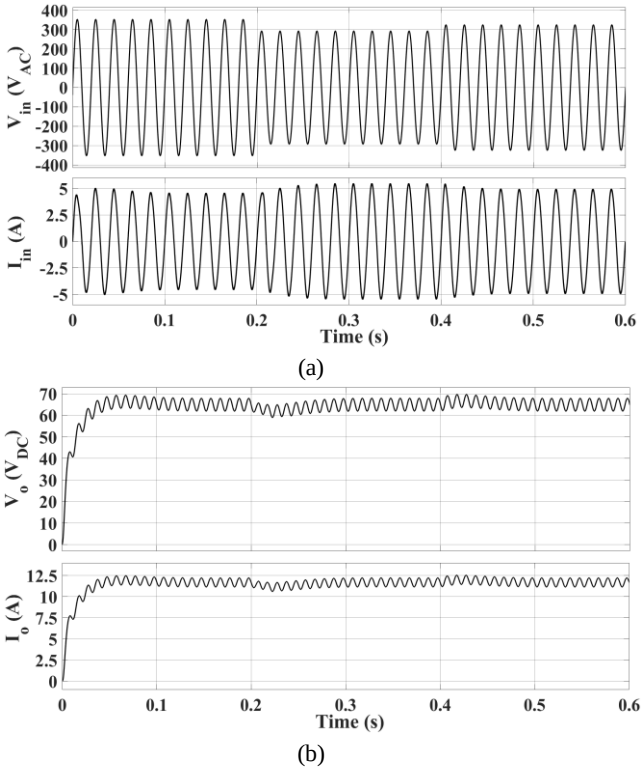

(a)

(b)

Figure 19. The input voltage fluctuation is applied to fuzzy, a) Input voltage and current, b) Output voltage and current

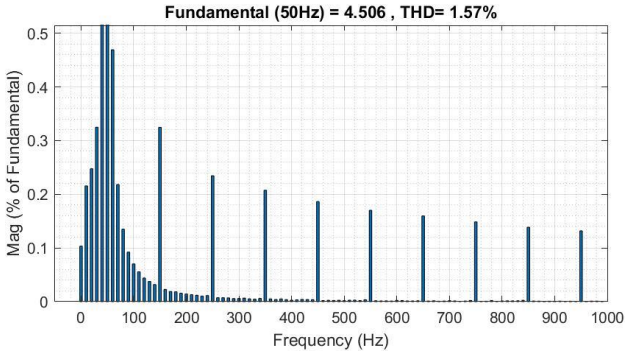

(a)

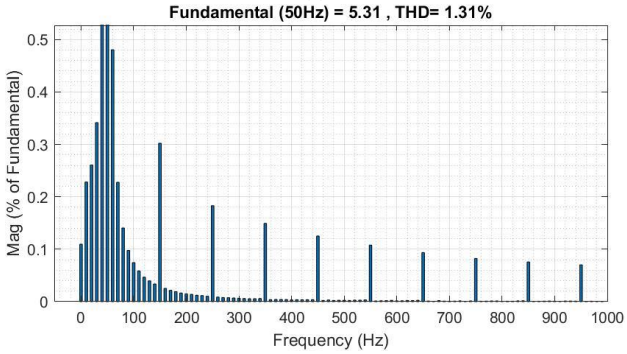

(b)

Figure 20. a) Transient THD when the input voltage is 253 V_{rms}, b) Transient THD when the input voltage is 207 V_{rms}

The fuzzy controller is also simulated for both the input voltage and output load fluctuation cases. The previously established range of input voltage fluctuation, which is in order of the maximum voltage of 253 V_{rms}, the minimum voltage of 207 V_{rms} and the nominal voltage of 230 V_{rms}, is implemented at the input of the BL SEPIC. The input current change is kept within the range of 5 ± 0.5 A by the fuzzy controller after the input voltage fluctuation range is applied. The full load of 12A is simulated at the output current. The output current fluctuation is observed in the range of 12 ± 1 A at the instant input voltage changes occurred. Furthermore, the output voltage is in the range of 65 ± 5 V, and the fluctuation at the output lasts less than 50 milliseconds. On the other hand, the reset function is inactive because no overshoot case is not observed by the PI voltage controller.

According to the input voltage fluctuation graphs, the maximum THD level of the fuzzy controller is 1.57 % when the input voltage is 253 V_{rms}. Also, the minimum THD is recorded as 1.31% for the 207 V_{rms}, as seen in Figure 20 (a) and Figure 20 (b). As a result, the input voltage fluctuations are suppressed by the PI controller, and the THD is within the limits that are specified in the standard.

The output voltage fluctuation case is simulated for fuzzy controller PFC operation as well. As shown in Figure 21, the BL SEPIC output is loaded with a full load of 12 A, a quarter load of 3 A and a half load of 6 A, respectively. After the full load is applied, the input current reaches 5 A of steady current within 50 milliseconds, as seen in Figure 21 (a). Then, an instant decrease of the output current from full load to quarter load is applied, and an overshoot is observed on the output voltage and current. However, the overshoot is suppressed by the PI voltage controller thanks to its reset feature. Because the output voltage exceeds the predefined 72 V_{dc} overshoot level, the reset feature is activated. Then, the half load of 6 A is applied to the fuzzy controller. Any overshoot is not observed as shown in Figure 21 (b), and a peak level of 2.5 A is observed at the input current.

The THD results of the fuzzy controller are given in Figure 22 (a) and Figure 22 (b). The minimum transient THD of 1.31% is obtained at the full load application. Moreover, the maximum transient THD of 3.10% is observed at the quarter load application. As a result, the controller again keeps the THD percents within the range of the standard.

By using the criteria shown in Table 4, both controller performances are compared with each other. The fuzzy controller reaches the targeted 65V output level faster than the PI controller, as shown in Figure 6 (b) and Figure 16 (b). The rise time of the PI controller is 28 milliseconds, and the output is settled at 38 milliseconds. Whereas the fuzzy has a 25 millisecond rise time, and the output is settled in 35 milliseconds. The PI controller overshoot is 1.34 % of the reference value. On the other hand, the fuzzy controller overshoots the reference output by 0.32 %.

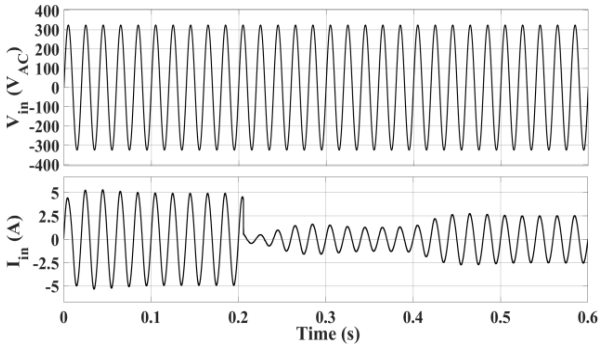

(a)

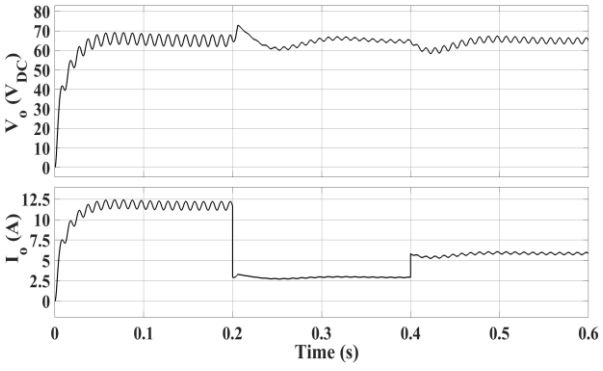

(b)

Figure 21. a) Input voltage and current of fuzzy controller when the output load fluctuation is applied, b) Output voltage and current of controller when the output load fluctuation is applied

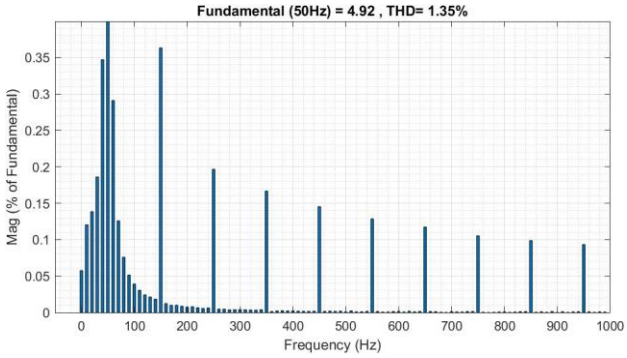

(a)

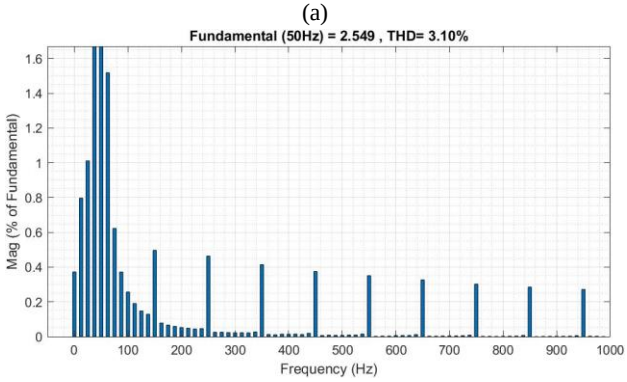

(b)

Figure 22. a) Transient THD result of fuzzy controller at full load, b) Transient THD result of fuzzy controller at quarter load

Even if the PI controller has better results for steady state operation with nominal input voltage and full load, the THD values of the fuzzy controller are better than the PI controller when simulating different input voltages and output loads. The THD results for output power changes are also given in Figure 24. The nonlinear structure of the fuzzy controller provides stable and robust control for the operational changes. The measured PF results that are given in Figure 25 are almost one for both PI and fuzzy controllers. As depicted in Figure 23, the maximum efficiencies of 93.5% and 93.4% are obtained with PI and fuzzy controllers, respectively.

The proposed topology features are also compared with similar BL topologies in the literature as given in Table 5 and Table 6. If the THD and PF performances of the topologies are compared, the BL CUK topology has the lowest steady state THD of 2.3 % with almost unity PF. The highest THD belongs to the BL Landsman topology with a unity PF. The minimum transient THD belongs to the BL zeta SEPIC with 1.8 %, and the maximum transient THD belongs to the BL boost converter. On the other hand, the proposed topology achieved steady state THD values of 1.08 % with the PI controller and 1.33 % with the fuzzy controller while the PF is almost unity. Moreover, the fuzzy controller has lower THD values for input voltage changes and the load changes. The proposed topology has also isolation, low input ripple and fewer complexity advantages. However, the proposed topology has medium efficiency among the compared topologies, high output ripple and discontinuous conduction mode (DCM) operation. The component counts of each topology are given in Table 6. The most complex topologies are the BL boost and BL landsman topologies due to their switching element and component numbers. In contrast, the BL CUK, BL totem pole and the proposed BL SEPIC are the least complex topologies.

Table 4. Comparison table of controllers

Properties	*PI*	*Fuzzy*
Rise time (ms)	28.08	24,96
Settling time (ms)	37.98	35,14
Overshoot (%)	1.34	0.32
Reaction	slower	faster
Simulation time	lower	higher
Calculation	complex	simple
Steady State THD (%)	1.08%	1.33%
Min transient THD (%)	1.64%	1.31%
Max transient THD (%)	3.25%	3.10%
Min power factor	0.999	0.999
Max efficiency (%)	93.5	93.4

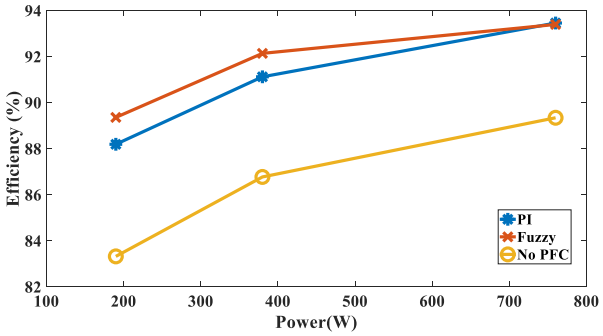

Figure 23. Efficiency results of PI, fuzzy and no PFC operation

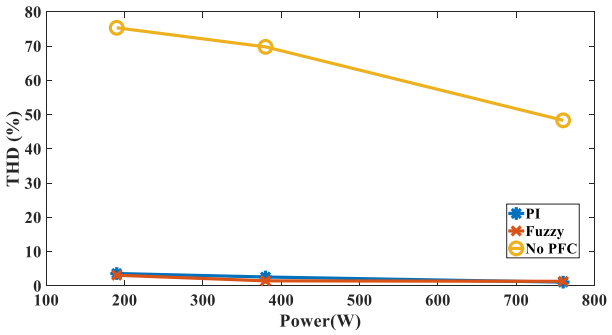

Figure 24. THD results of PI, fuzzy and no PFC operation

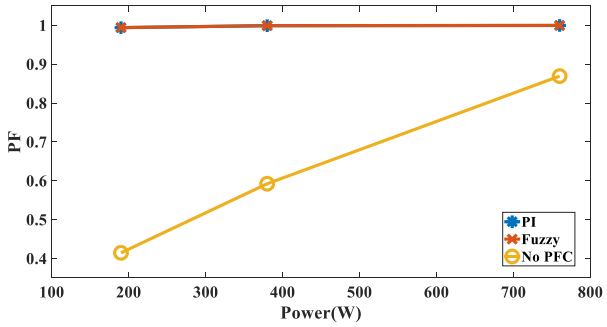

Figure 25. PF results of PI, fuzzy and no PFC operation

Table 5. Comparison table of different BL topologies

Topology	BL Boost [24]	BL Buck Boost [24]	BL Landsman [25]	BL CUK [24]	BL Zeta SEPIC [26]	BL SEPIC [27]	BL SEPIC [38]	Proposed With PI Controller	Proposed With Fuzzy Controller
MOSFET Voltage Stress	High	High	High	Low	High	Low	Low	Low	Low
MOSFET Current Stress	Low	High	High	High	Low	High	High	High	High
Input Ripple	Low	Low	Low	Low	Low	Low	Low	Low	Low
Output Ripple	Low	Low	High	Low	Low	High	High	High	High
Isolation	No	Yes	Yes	No	Yes	No	Yes	Yes	Yes
Operation Mode	CCM	DCM	CCM	DCM	DCM	DCM	DCM	DCM	DCM
Max Efficiency (%)	98.9	82	91	94	92	93.3	92.3	93.5	93.4
Rated Power (VA)	3400	856	885	1000	878	453	762	760	760
Steady State THD (%)	<5	3.5	4.8	3.49	2.3	4.0	1.55	1.08	1.33
Min Transient THD (%)	3.5	2.3	4.3	3.49	1.8	2.7	2.32	1.64	1.31
Max Transient THD (%)	41	3.5	4.8	3.88	<5	5.2	5,8	3.25	3.1
PF	0.99	1	1	0.9994	1	0.99	1	0.999	0.999

Table 6. Comparison table of different BL topologies

Topology	Number of Components						Total	Complexity	Cost
	L	Tr	C	Sw	D	Rl			
BL Boost [24]	4	0	1	4	4	0	13	Medium	~39.3$
BL Buck Boost [24]	3	1	3	3	5	0	15	High	-
BL Landsman [25]	5	1	5	3	5	0	18	High	~74.1$
BL CUK [24]	2	0	3	2	2	0	9	Low	~74.7$
BL Zeta SEPIC Flyback [26]	3	1	4	3	3	0	14	Medium	-
BL SEPIC [27]	3	0	2	2	4	0	11	Low	-
BL SEPIC [38]	1	2	3	2	2	0	10	Low	-
Proposed	1	2	3	2	2	0	10	Low	-

Note: L: Inductor, Tr: Transformer, C: Capacitor, Sw: Switch, D: Diode, Rl: Relay

4. Conclusion

In this study, BL SEPIC is introduced to reduce THD more effectively than traditional bridge rectifiers. Then, the PI and fuzzy controllers are compared using the BL SEPIC converter. Even if the fuzzy controller has a faster response time than the PI controller, simulating the fuzzy controller requires much more computational effort. However, the calculations for the fuzzy controller are less complex because a mathematical model of the system is required for the PI controller to calculate P and I coefficients correctly, whereas the fuzzy controller merely needs language qualifiers to create input and output relations.

The comparison of PFC operation for both controllers is obtained from the simulation results. The PI and fuzzy controllers have minimum steady state THD values of 1.08% and 1.33%, respectively. However, the BL SEPIC is also simulated to see the transient performance of the controllers. Initially, the input voltage fluctuations are applied to the controllers. The results show that the PI controller has a minimum of 1.64% transient THD, while the fuzzy controller has 1.31% transient THD. Finally, the output load variation is applied. It is seen that the PI controller has a maximum of 3.25% transient THD, while the fuzzy controller has 3.10% transient THD. As a result, the THD performance of controllers complies with IEC 61000-3-2:2018 requirements. On the other hand, the fuzzy controller demonstrated better operation for input voltage and load current changes. Therefore, the fuzzy controller is a more stable and robust method as compared with the PI controller method. Also, the obtained THD values are within the

standard voltage limits of < 5% that is specified in IEC 60038:2009. The THD and PF requirements in regulations and standards provide increasing power quality for grid connected devices such as EV chargers. The upcoming future may lead to up-to-date regulations such as more strict PFC operation, power efficiency, or device performance due to the increasing need for power. Therefore, the following studies are listed below as future scope of the proposed work.

- The fuzzy controller can be simulated with other BL converters to investigate their PFC performance with non-linear systems.
- The simulated results can also be implemented in a practical application to see the practical PFC performance. Also, efficiency can be increased by using GaN or SiC based semiconductors.
- Several other non-linear control methods such as sliding mode control and model predictive control can be implemented in the bridgeless topologies for further performance enhancement and comparisons.

Declaration

The author(s) declared no potential conflicts of interest with respect to the research, authorship, and/or publication of this article. The author(s) also declared that this article is original, was prepared in accordance with international publication and research ethics, and ethical committee permission or any special permission is not required.

Author Contributions

The study is supervised by A. Karaarslan. The control algorithms and the proposed topology are implemented and simulated in MATLAB Simulink by A. Uğurluoğlu. The manuscript was written by A. Uğurluoğlu and controlled by A. Karaarslan.

References

1. Drobnič, K., G. Grandi, M. Hammami, R. Mandrioli, A. Viatkin, and M. Vujacic, *A ripple-free dc output current fast charger for electric vehicles based on grid-tied modular three-phase interleaved converters.* In 2018 International symposium on industrial electronics (INDEL), 2018. p.1-7.
2. Ajanovic, A., and R. Haas, *Economic and environmental prospects for battery electric-and fuel cell vehicles: a review*. Fuel cells, (2019). **19**(5): p.515-529.
3. Rahman, S., I. A. Khan, and M. H. Amini, *A review on impact analysis of electric vehicle charging on power distribution systems.* In 2020 2nd International Conference on Smart Power & Internet Energy Systems (SPIES), IEEE, 2020, p. 420-425.
4. Koç, M., O. B. Tör, and Ş. Demirbaş, *Analysis the Effects of Electric Vehicles on Distribution Networks with Simulations Based on Probabilistic Methods.* Gazi University Journal of Science Part C: Design and Technology, 2021. **9**(1): p.95-107.
5. Akın, Ö., İ. Özer, and H. Ünlü, *Selective harmonic elimination in multi-level inverters by using neural networks.* International Advanced Researches and Engineering Journal, 2021. **5**(1): p.19-25.
6. Das, P., M. Pahlevaninezhad, J. Drobnik, G. Moschopoulos, and P. K. Jain, *A nonlinear controller based on a discrete energy function for an AC/DC boost PFC converter.* IEEE Transactions on Power Electronics, 2013. **28**(12): p.5458-5476.
7. Pena-Alzola, R., M. A. Bianchi, and M. Ordonez, *Control design of a PFC with harmonic mitigation function for small hybrid AC/DC buildings.* IEEE Transactions on Power Electronics, 2015. **31**(9): p.6607-6620.
8. *Limits for Harmonic Current Emissions (Equipment Input Current up to and Including 16A Per Phase)*. IEC Std. 61000-3-2, 2020.
9. Karaman, Ö. A., A. Gündoğdu, and M. Cebeci, *Performing reactive power compensation of three-phase induction motor by using parallel active power filter.* International Advanced Researches and Engineering Journal, 2020. ***4***(3): p.239-248.
10. Musavi, F., M. Edington, W. Eberle, and W. G. Dunford, *Evaluation and efficiency comparison of front end AC-DC plug-in hybrid charger topologies.* IEEE Transactions on Smart grid, 2011. **3**(1): p.413-421.
11. Valascho, R., and S. Abdel-Rahman, *Digital PFC CCM boost converter*. Infineon Technologies, Application Note, Munich, Germany, 2016.
12. Kalair, A., N. Abas, A. R. Kalair, Z. Saleem, and N. Khan, *Review of harmonic analysis, modeling and mitigation techniques.* Renewable and Sustainable Energy Reviews, 2017. **78**: p.1152-1187.
13. Jang, Y., and M. M. Jovanović, *Bridgeless high-power-factor buck converter.* IEEE Transactions on Power Electronics, 2010. **26**(2): p.602-611.
14. Jang, Y., and M. M. Jovanovic, *A bridgeless PFC boost rectifier with optimized magnetic utilization.* IEEE Transactions on Power Electronics, 2009. **24**(1): p.85-93.
15. Zhao, B., A. Abramovitz, and K. Smedley, *Family of bridgeless buck-boost PFC rectifiers.* IEEE Transactions on Power Electronics, 2015. **30**(12): p.6524-6527.
16. Akhtar, M. F., S. R. S. Raihan, N. A. Rahim, M. N. Akhtar and E. Abu Bakar, *Recent developments in DC-DC converter topologies for light electric vehicle charging: a critical review.* Applied Sciences, 2023. ***13***(3): p.1676.
17. Kushwaha, R., B. Singh and V. Khadkikar, *An improved PQ Zeta converter with reduced switch voltage stress for electric vehicle battery charger.* In 2020 IEEE Energy Conversion Congress and Exposition (ECCE), 2020, October. p. 858-863. IEEE.
18. Gupta, J., R. Kushwaha and B. Singh, *An Isolated Improved Power Quality Battery Charger for a Light Electric Vehicle.* In 2020 IEEE International Conference on Power Electronics, Smart Grid and Renewable Energy (PESGRE2020), 2020, January, p. 1-6. IEEE.
19. Samsudin, N. A., D. Ishak, and A. B. Ahmad, *Design and experimental evaluation of a single-stage AC/DC converter with PFC and hybrid full-bridge rectifier.* Engineering science and technology, an international journal, 2018. **21**(2): p.189-200.
20. Jeong, S. G., J. M. Kwon, and B. H. Kwon, *High-efficiency bridgeless single-power-conversion battery charger for light electric vehicles.* IEEE Transactions on Industrial Electronics, 2018. **66**(1): p.215-222.
21. Pandey, R., and B. Singh, *PFC-SEPIC converter-fed half-*

bridge LLC resonant converter for e-bike charging applications. IET Electrical Systems in Transportation, 2020. **10**(3): p.225-233.

22. Zhou, K., H. Yang, Y. Zhang, Y. Che, Y. Huang and X. Li, *A review of the latest research on the topological structure and control strategies of on-board charging systems for electric vehicles.* Journal of Energy Storage, 2024. *97*: 112820.
23. Onal, Y., *Analysis of a new SEPIC AC–DC PFC converter for light emitting diode applications.* Emerging Materials Research, 2021. **11**(1): p.51-59.
24. Dutta, S., S. Gangavarapu, A. K. Rathore, R. K. Singh, S. K. Mishra and V. Khadkikar, *Novel single-phase Cuk-derived bridgeless PFC converter for on-board EV charger with reduced number of components*. IEEE Transactions on Industry Applications, 2022. ***58***(3): p.3999-4010.
25. Kushwaha, R. and B. Singh, *Power factor improvement in modified bridgeless landsman converter fed EV battery charger.* IEEE transactions on Vehicular Technology, 2019. ***68***(4): p.3325-3336.
26. Kushwaha, R. and B. Singh, *Power factor correction in EV charger with bridgeless Zeta-SEPIC converter.* In 2019 IEEE Energy Conversion Congress and Exposition (ECCE), 2019, September, p.121-128. IEEE.
27. Gupta, J., R. Kushwaha, B. Singh and V. Khadkikar, *Improved power quality charging system based on high step-down gain bridgeless SEPIC APFC for light electric vehicles.* IEEE Transactions on Industry Applications, 2021. **58**(1): p.423-434.
28. Çamur, H., Z. Ortatepe and A. Karaarslan, *Comparative Analysis of Current Control Methods Implemented in Single-Phase Boost PFC Converter in CCM Mode*. International Scientific Research and Innovation Congress-ISARC, İstanbul, Turkey, 2022. p.984-992.
29. Gupta, M., N. Gupta, M. M. Garg and A. Kumar, *Robust control strategies applicable to DC–DC converter with reliability assessment: A review*. Advanced Control for Applications: Engineering and Industrial Systems, 2024. ***6***(3): p.217.
30. Mumtaz, F., N. Z. Yahaya, S. T. Meraj, B. Singh, R. Kannan and O. Ibrahim, *Review on non-isolated DC-DC converters and their control techniques for renewable energy applications.* Ain Shams Engineering Journal, 2021. ***12***(4): p.3747-3763.
31. Aldemir, A. and M. S. Anwer, *Determination of optimal PID control parameters by response surface methodology*. International Advanced Researches and Engineering Journal, 2020. ***4***(2): p.142-153.
32. Hitit, Z. Y., İ. Koçer, G. Kuş, N. Z. Arslan, E. P. Dal and H. Koz, *Optimal PID control with anti-windup in neutralization process.* International Advanced Researches and Engineering Journal, 2023. ***7***(3): p.138-145.
33. Sundaramoorthy, S., M. G. Umamaheswari, G. Marimuthu and B. Lekshmisree, *Hopfield neural network-based average current mode control of synchronous SEPIC converter*. IETE Journal of Research, 2023. ***69***(6): p.3897-3915.
34. Durgadevi, S. and M. G. Umamaheswari, *Analysis and design of single phase power factor correction with DC–DC SEPIC Converter for fast dynamic response using genetic algorithm optimised PI controller.* IET Circuits, Devices & Systems, 2018. ***12***(2): p.164-174.
35. Xia, B., Y. Li, G. Zhang, Q. Cheng and F. Ding, *A double-layer ring-structured equalizer for series-connected lithium-ion battery pack based on model predictive control.* Journal of Energy Storage, 2024. ***78****:* p.110047.
36. Sezen, A. and K. Keskin, *Hybrid Control of DC-DC Buck Boost Converter*. Demiryolu Mühendisliği, 2021. (14): p.99-109.
37. Köseoğlu, E. and A. Karaarslan, *Modified Bi-Directional Cuk Converter For Cell Balancing Using PI And Fuzzy Logic Control Method.* Journal of Optimization and Decision Making, 2023. ***2***(2): p.283-289.
38. Singh, B., and R. Kushwaha, *A PFC based EV battery charger using a bridgeless isolated SEPIC converter*. IEEE Transactions on Industry applications, (2019). **56**(1): p.477-487.
39. Kunjittipong, N., K. Kongkanjana, and S. Khwan-on, *Comparison of fuzzy controller and PI controller for a high step-up single switch boost converter.* In 2020 3rd International Conference on Power and Energy Applications (ICPEA), IEEE, 2020. p. 94-98
40. *Voltages*, I. S. Iec standard iec 60038. Ed, 2009.
41. ALKAN, Ö., S. TOSUN and Ö. ALKAN, *Enerji Kalitesi Açısından Harmonikli Bir Sağlık Tesisinin İncelenmesi.* Düzce Üniversitesi Bilim ve Teknoloji Dergisi, 2019. **7**(1): p.709-721.
42. Marti, J. V., *Analysis of duty cycle to output voltage transfer functions of cúk-like class dc-dc converters.* In Annual Seminar on Automation, Industrial Electronics and Instrumentation, 2015.
43. Sevim, D., and V. Gider, *Designing a Control Interface and PID Controller of CUK Converter*. European Journal of Technique (EJT), 2021. **11**(1): p.93-100.
44. Anusiya, K., and K. Ramadas, *SEPIC converter based transformer less grid tied PV system with reactive power compensation.* In 2017 IEEE International Conference on Intelligent Techniques in Control, Optimization and Signal Processing (INCOS), 2017. p.1-7.
45. Çamur, H., Z. Ortatepe, and A. Karaarslan, *Fuzzy logic control based dual input boost converter.* 4. International Scientific Research and Innovation Congress, İstanbul, Turkey, 2022. p.993-1002.